# Radar Rain-Rate Estimators and Their Variability due to Rainfall Type: An Assessment Based on Hydrometeorology Testbed Data from the Southeastern United States

SERGEY Y. MATROSOV

*Cooperative Institute for Research in Environmental Sciences, University of Colorado, and Physical Sciences Division, NOAA/Earth System Research Laboratory, Boulder, Colorado*

ROBERT CIFELLI, PAUL J. NEIMAN, AND ALLEN B. WHITE

*Physical Sciences Division, NOAA/Earth System Research Laboratory, Boulder, Colorado*

(Manuscript received 1 October 2015, in final form 7 March 2016)

ABSTRACT

S-band profiling (S-PROF) radar measurements from different southeastern U.S. Hydrometeorology Testbed sites indicated a frequent occurrence of rain that did not exhibit radar bright band (BB) and was observed outside the periods of deep-convective precipitation. This common nonbrightband (NBB) rain contributes ~15%–20% of total accumulation and is not considered as a separate rain type by current precipitation-segregation operational radar-based schemes, which separate rain into stratiform, convective, and, sometimes, tropical types. Collocated with S-PROF, disdrometer measurements showed that drop size distributions (DSDs) of NBB rain have much larger relative fractions of smaller drops when compared with those of BB and convective rains. Data from a year of combined DSD and rain-type observations were used to derive S-band-radar estimators of rain rate $R$, including those based on traditional reflectivity $Z_e$ and ones that also use differential reflectivity $Z_{\mathrm{DR}}$ and specific differential phase $K_{\mathrm{DP}}$. Differences among same-type estimators for mostly stratiform BB and deep-convective rain were relatively minor, but estimators derived for the common NBB rain type were distinct. Underestimations in NBB rain-rate retrievals derived using other rain-type estimators (e.g., those for BB or convective rain or default operational radar estimators) for the same values of radar variables can be on average about 40%, although the differential phase-based estimators are somewhat less susceptible to DSD details. No significant differences among the estimators for the same rain type derived using DSDs from different observational sites were present despite significant separation and differing terrain. Identifying areas of common NBB rain could be possible from $Z_e$ and $Z_{DR}$ measurements.

## 1. Introduction

Errors of radar-based quantitative precipitation estimation (QPE) at the ground are caused by a number of different factors, including radar calibration uncertainties, partial beamfilling and blockage, vertical changes in observed variables between radar resolution volumes and the ground, and variability in drop size distributions (DSDs) that modify mean relations between rainfall and radar variables. The DSD variability results in changes in relations between rain rate $R$ and the equivalent radar reflectivity factor on horizontal polarization $Z_{eh}$ (hereinafter, just reflectivity $Z_e$), which are used in the traditional radar-based QPE methods and also in relations that additionally utilize polarimetric radar variables such as differential reflectivity $Z_{\mathrm{DR}}$ and the specific differential phase shift $K_{\mathrm{DP}}$ (e.g., Bringi and Chandrasekar 2001).

For the continental United States, the Multi-Radar Multi-Sensor (MRMS) system, which was built using components of the National Mosaic and Multi-Sensor QPE (NMQ) system and which utilizes National Weather Service ground-based scanning S-band (~3 GHz) Weather Surveillance Radar-1998 Doppler (WSR-88D) measurements, uses several default $Z_e$–$R$ relations (e.g., Zhang et al. 2011), including those for convective rain ($Z_e = 300R^{1.4}$; $Z_e$ is in $\mathrm{mm^6\,m^{-3}}$ and $R$ is in millimeters per hour), stratiform rain ($Z_e = 200R^{1.6}$),

*Corresponding author address*: Sergey Y. Matrosov, R/PSD2, 325 Broadway, Boulder, CO 80305.
E-mail: sergey.matrosov@noaa.gov

DOI: 10.1175/JAMC-D-15-0284.1

and warm "tropical" rain ($Z_e = 230R^{1.25}$). The stratiform WSR-88D relation is often referred to as the Marshall–Palmer relation (Marshall et al. 1955). Snowflake melting is one of the dominant mechanisms for stratiform-rainfall formation, and this rainfall type typically exhibits the radar bright band caused by mixed-phase hydrometeors in the melting layer. The convective WSR-88D relation represents the "Miami" relation from Woodley (1970). The $Z_e = 230R^{1.25}$ relation, which is based on observed tropical rainfall DSDs, was proposed for C-band (~5 GHz) frequencies by Rosenfeld et al. (1993) for monsoon, convective maritime rain regimes, and continental squall lines. Algorithms that are based on radar measurements were developed (e.g., Qi et al. 2013) to segregate observed rainfall into either stratiform or convective type so that a corresponding $Z_e$–$R$ relation can be applied. Rain-rate estimators that use polarimetric radar variables are also expected to be sensitive to rainfall type, although this sensitivity has yet to be assessed in relative detail.

NOAA's Hydrometeorology Testbed (HMT) program maintains ground-based sites that provide essential meteorological and hydrological observations. Some of these sites are equipped with vertically pointing S-band (~3 GHz) profilers (S-PROFs), which provide 60-m vertical resolution reflectivity and Doppler velocity profiles. The averaging time for one profile is typically about 1–1.3 min (depending on the S-PROF configuration). The S-PROF measurements allow a robust classification of precipitation types, including brightband (BB) stratiform-like rainfall, nonbrightband (NBB) rainfall, and also an NBB-rainfall portion representing deep convection, which generally corresponds to convective rain according to operational radar-based segregation algorithms (e.g., Qi et al. 2013). Different aspects of the S-PROF-based rainfall-type classification scheme are given by White et al. (2003). The only subjective part of this scheme is identifying deep-convective rainfall. For the purpose of this study, the BB rain classified using this scheme is considered a single category without subdividing it into smaller subcategories [e.g., a "hybrid" BB-rain subcategory as in White et al. (2003)] depending on the reflectivity slope below the melting layer. In the dataset used in this study, BB rain with a general increase of reflectivity toward the ground contributed ~95% of the total BB-rain accumulation.

Earlier studies utilizing one winter season of data from coastal sites in California from the HMT-West (Martner et al. 2008) program (http://hmt.noaa.gov) indicated that a significant portion of total precipitation that results in NBB rainfall is characterized by DSDs that differ markedly from those of BB stratiform-like rainfall. Relative to BB rainfall, NBB rainfall contained larger fractions of smaller drops, which was likely (as these authors suggested) due to orographically forced hydrometeor growth processes. The corresponding NBB-rain $Z_e$–$R$ relations derived for coastal HMT-West areas were very different from default WSR-88D relations. The results of the study by Martner et al. (2008) were based on radar-profiler and collocated DSD measurements at two coastal HMT-West sites.

The main objective of this study is to investigate the influence of rainfall types on S-band $Z_e$–$R$–based and polarimetric rain-rate estimators using collocated S-PROF-based rain-type differentiation and collocated DSD measurements conducted at the HMT southeastern sites located in mountainous and flat-terrain environments in North Carolina. The HMT southeastern sites were deployed as part of the HMT-Southeast Pilot Study (HMT-SEPS), aimed at identifying leading sources of error in quantitative precipitation forecasts (QPF) and QPE in this region. Other goals of this study are to provide information on occurrences over the annual cycle and intensities of different rain types and to evaluate the possibility of distinguishing between BB and NBB rain observed outside the deep-convection periods on the basis of WSR-88D polarimetric measurements. The term "common NBB rain" is hereinafter used in this study for this NBB rain type that excludes deep-convective rain, which is typically characterized by high-reflectivity cores (~30–35 dB$Z$) above the freezing level.

## 2. Observational sites and datasets

Data from two HMT-SEPS sites in North Carolina were collected using the S-PROF radars and collocated ground-based disdrometers, tipping-bucket rain gauges, and standard surface meteorological instruments. One site was located near New Bern (EWN) in a coastal location [35.078°N, 77.046°W; 3 m above mean sea level (MSL)] with flat terrain surrounding it. The other site at Old Fort (OFT) was located ~470 km west-northwest of EWN in a mountainous region of the Appalachian foothills (35.643°N, 82.161°W; 427 m MSL). The HMT site at Hankins (HKS), located near OFT, lacked an S-PROF radar but had disdrometer and standard meteorological measurements. The general area of the HMT-Southeast has nine WSR-88D systems (see Fig. 1).

Rainfall at EWN and OFT was observed by quality-controlled Particle Size and Velocity (Parsivel) optical disdrometers (Löffler-Mang and Joss 2000) that recorded DSD spectra every 2 min. An annual cycle of the observed rainfall data (10 August 2013–9 August 2014) is used in this study, although the OFT Parsivel malfunctioned from 30 May to 9 July 2014 (the

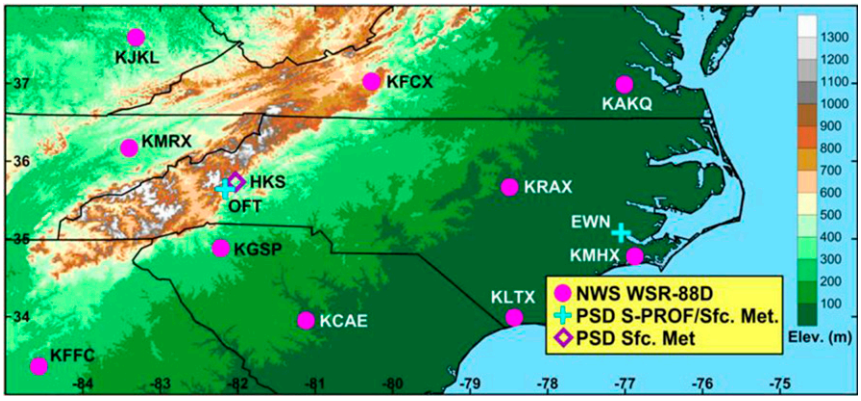


FIG. 1. A map showing the EWN, OFT, and HKS HMT-SEPS Physical Sciences Division (PSD) observational sites and locations of nearby WSR-88D units.

corresponding data were not used). Rare snowfall and mixed-phase precipitation data observed at OFT and EWN were excluded from the analysis.

Rainfall accumulations for individual events derived from the Parsivel disdrometer DSD spectra and collocated standard tipping-bucket-type meteorological gauges were generally in agreement to within 10%–15%. A close agreement of Parsivel rain-rate retrievals and those from robust 2D-video-disdrometer measurements (at least for not-very-heavy rainfall for which large and nonfully melted hydrometeors can be present) was also noted by Thurai et al. (2011). It provides an additional indication for suitability of the Parsivel disdrometer data in deriving rain rates that are approximately proportional to the 3.7th DSD moment for drops smaller than approximately 3.5 mm (e.g., Matrosov 2005). While smaller-drop parameter estimates from Parsivel disdrometers (especially for the older disdrometer models) are generally less reliable than those for larger-drop estimates (Löffler-Mang and Joss 2000), uncertainties of their contribution to the higher DSD moments (i.e., rain rate and especially reflectivity, which is proportional to the sixth DSD moment for frequencies considered in this study) are not expected to be crucial.

S-PROF vertically pointing measurements were used to classify rain types in half-hour periods on the basis of profile-by-profile analysis using the technique described by White et al. (2003). If several different rain types were observed during a particular 30-min period, the rain type with more clearly defined profiles was assigned to the entire half-hour period. An example of the EWN S-PROF measurements for 27–28 June 2014 is shown in Fig. 2. Periods of BB and common NBB rain are observed during the last three hours on 27 June 2014 and between approximately 1500 and 1700 UTC on 28 June 2014, respectively. Prior to BB rain on 27 June 2014, a heavy convective-core shower is observed between around 1800 and 1920 UTC. This shower is

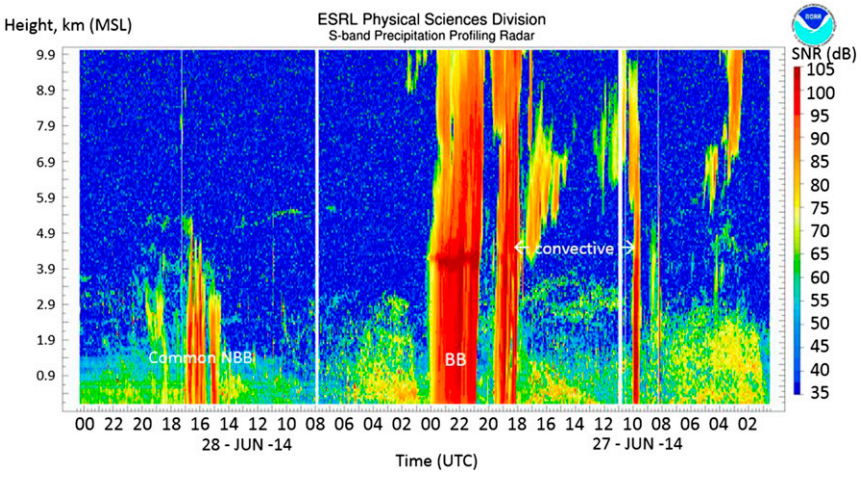


FIG. 2. An example of S-PROF observations on 27–28 Jun 2014 at EWN. Different types of rain are seen as described in the text. Note that time in the figure progresses from right to left.

TABLE 1. Total accumulations and mean rain rates and reflectivities at the EWN and OFT sites for different types of rain according to the Parsivel and gauge data.

| Rain type | BB rain | Convective | NBB common |
|---|---|---|---|
| EWN Parsivel/gauge 10 Aug 2013–9 Aug 2014 | 465 mm/470 mm | 435 mm/394 mm | 163 mm/149 mm |
| OFT Parsivel/gauge 10 Aug 2013–9 Aug 2014, excluding 30 May 2013–9 Jul 2014 | 605 mm/625 mm | 89 mm/103 mm | 159 mm/174 mm |
| OFT gauge 30 May 13–9 Jul 14 | 36 mm | 169 mm | 61 mm |
| EWN Parsivel mean $R$ and $Z_e$ | 3.2 mm $h^{-1}$; 34.0 dB$Z$ | 13.3mm $h^{-1}$; 43.1 dB$Z$ | 3.8 mm $h^{-1}$; 31.2 dB$Z$ |
| OFT Parsivel mean $R$ and $Z_e$ | 3.6 mm $h^{-1}$; 34.2 dB$Z$ | 13.6mm $h^{-1}$; 43.3 dB$Z$ | 3.5 mm $h^{-1}$; 30.5 dB$Z$ |

characterized by the lack of a pronounced bright band and strong radar echo cores observed above the environmental freezing level, which for this event was located at ~4.4 km MSL (i.e., ~200 m above the middle of the bright band). Although radar echoes for common NBB rain observed on 28 June 2014 do not extend very high, which suggests the dominance of warm-rain processes, sometimes echo tops of this rain type can be noticeably higher than the environmental freezing level (e.g., Matrosov et al. 2014). The convective-core rainfall, which is specifically segregated in the WSR-88D-based QPE schemes, and common NBB rain, which is usually not considered as a distinct rain type by the radar-based QPE algorithms, lack an identifiable radar bright band.

Table 1 presents the total accumulations and mean rain rates and S-band reflectivities inferred from disdrometer measurements at the EWN and OFT sites for different rain types as classified using the S-PROF measurements. The total amounts of rainfall during the annual period between 10 August 2013 and 9 August 2014 were similar at both sites (~1000–1200 mm), with a little more (less) than one-half of the total resulting from BB rain at OFT (EWN). Similar fractions of BB rain in total rainfall accumulations were also observed during precipitation associated with cool-season atmospheric river landfalls at the California coast (Matrosov et al. 2014). When compared with HMT-West, deep-convective rain at the HMT-SEPS sites contributes more significantly to the totals, with a noticeably higher fraction at the coastal site (i.e., ~38% and 23% of total accumulations at the EWN and OFT sites, respectively). Contributions of common NBB rain, which is observed more often than convective rain, are also significant (i.e., ~15% and 20% of total accumulations at EWN and OFT, respectively).

Microphysical differences among different rain types are evident in Fig. 3, which shows their mean DSDs as a function of the Parsivel bin size. These DSD representations were obtained by averaging drop counts for each disdrometer size bin while accounting for the bin width. All observed DSDs for a given rain type resulting in S-band $Z_e$ of greater than 15 dB$Z$ were used for calculating mean DSDs. This reflectivity threshold roughly corresponds to precipitation rates of 0.3–0.5 mm $h^{-1}$, which are typically associated with moderate to heavier drizzle (Huschke 1959). Although BB rain and common NBB rain have similar mean intensities ($R$ of ~3.5 mm $h^{-1}$), the former rain type, as seen from Fig. 3, is typically characterized by a significantly smaller (greater) relative fraction of small (large) drops than the latter one (even though Parsivel smaller-drop counts might be underestimated). This distinction results in differing typical reflectivities of these rain types, with mean $Z_e$ values for BB rain being higher when compared with common NBB rain of similar rain rate.

Deep-convective NBB rain (hereinafter, just convective rain) at both observational sites is more intense, although general shapes of BB and convective-rain drop size spectra are somewhat similar (except for larger drop counts in convective rain). Even though some rain (especially convective rain) was missed during the 40-day OFT Parsivel outage period, all particular rain-type (i.e., BB, common NBB, and convective NBB rain) mean DSDs are in close agreement at both sites in terms of

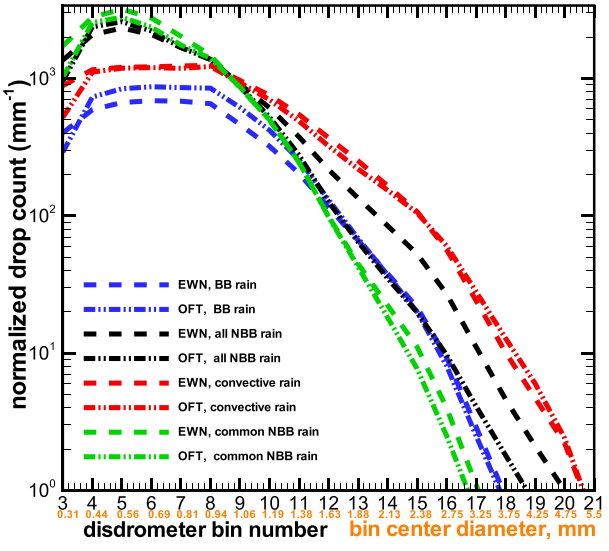


FIG. 3. Mean DSDs observed at the HMT-Southeast OFT and EWN sites for different types of rain during a 1-yr period between 10 Aug 2013 and 9 Aug 2014.

drop spectra shape and counts (see Fig. 3). This agreement suggests a similarity of rainfall formation processes for a given rain type, despite the fundamentally different geographic characteristics at these two sites. The differences in the mean EWN and OFT DSDs for combined NBB rain, which includes convective and common NBB parts, are due to differing convective-rain fractions at these sites.

Disdrometer-derived DSDs are used in this study for obtaining $Z_e$–$R$ relations and polarimetric rain-rate estimators in the next sections. Utilizing measured DSDs without fitting observations by analytical functions such as the gamma function, which is often used for describing raindrop DSDs, provides a more direct way of developing QPE approaches since it avoids uncertainties caused by fitting experimental data to approximately match predetermined functional shapes. Also, several recent studies (e.g., Adirosi et al. 2014, 2015; Ekerete et al. 2015) have questioned the adequacy of the gamma-function distribution for representing the natural variability of DSDs.

## 3. Reflectivity-based rain-rate estimators for different rain types

Figure 4 shows scatterplots of S-band reflectivity (assuming a beam tilt of 0.5°) versus rain rate as derived from the yearlong Parsivel DSD measurements at different HMT-SEPS sites. DSD-based calculations allow for concurrent high-temporal-resolution (~2 min) estimates of different radar variables and rain rates. The **T**-matrix calculations (e.g., Waterman 1965) and the spheroidal-drop-shape mean aspect ratio model from Brandes et al. (2005) were used for calculating radar variables using observed DSD spectra. In addition to the S-PROF locations at EWN and OFT, the data are shown also for the HKS site that is located just 15 km from the OFT site in similar terrain (see Fig. 1). The lack of an S-PROF at the HKS site precluded rain-type differentiation at that site. The all-rain-data scatterplots and best $Z_e$–$R$ relations at HKS and OFT, however, are very close, which supports an assumption that the OFT Parsivel outage period did not significantly affect the overall DSD statistics at this site. The mean all-rain $Z_e$–$R$ relations for OFT and HKS are also close to that at the EWN coastal site despite the differing terrain and the ~470-km separation.

Since the S-PROF measurements at EWN and OFT provided rain-type partitioning, $Z_e$–$R$ relations for different rain types could be derived using DSDs measured at these sites. These relations are shown in Table 2 and Fig. 5. They were derived using a customary power-law least squares regression approach assuming $Z_e$ as an independent variable but are presented in a traditional form (i.e., $Z_e = aR^b$). It can be seen that relations for the same rain type at both EWN and OFT are similar. For BB, NBB common, and convective rains these relations at both sites provide rain-rate estimates that are mostly within about 20%, 10%, and 12%, respectively, when reflectivities vary in the 15–53-dB$Z$ range (note that a

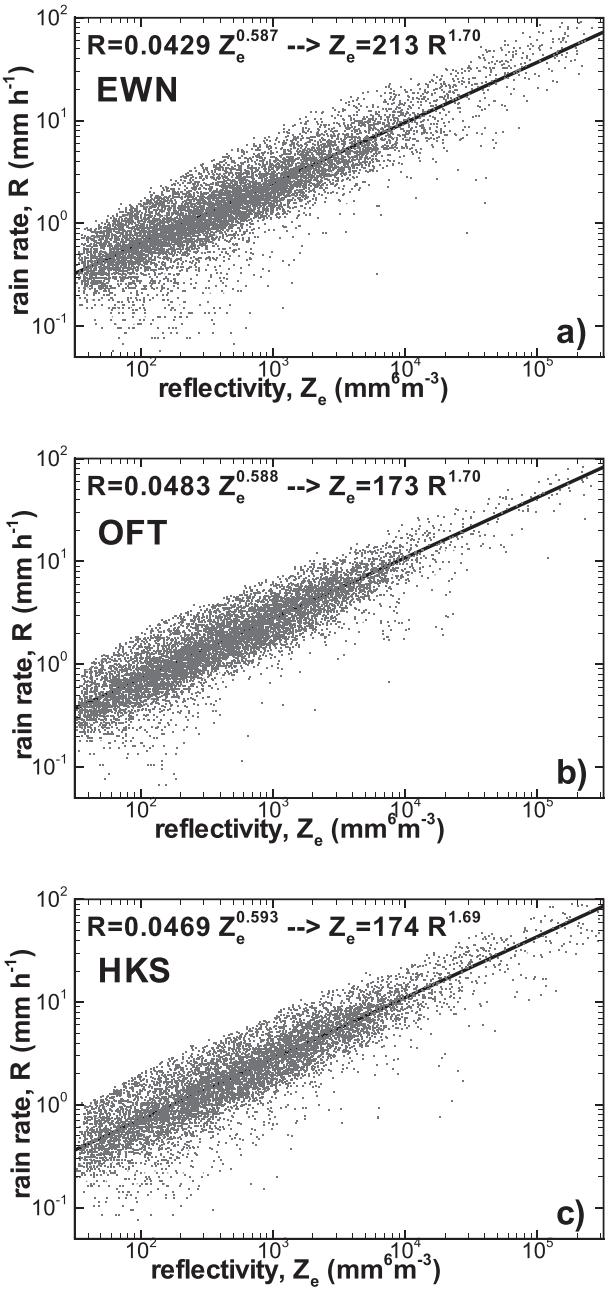


FIG. 4. The $Z_e$–$R$ scatterplots for all rain data as based on the Parsivel DSD measurements that resulted in $Z_e > 15$ dB$Z$ at the (a) EWN, (b) OFT, and (c) HKS sites.

TABLE 2. S-band $Z_e = aR^b$, $R = cZ_e^dZ_{dr}^f$, $Z_{DR} = pZ_e^u$, and $R = gK_{DP}^h$ relations and the NMAD characterizing different rain-rate estimators derived from disdrometer DSDs for four different rain types at three HMT-Southeast sites ($R$ is in millimeters per hour, $Z_e$ is in mm$^6$ m$^{-3}$ except that in the $Z_{DR}$–$Z_e$ relations $Z_e$ is in units of "dBZ," $K_{DP}$ is in degrees per kilometer, $Z_{DR}$ is in decibels, and $Z_{dr}$ is dimensionless). The Brandes et al. (2005) drop axis ratio–size relation was assumed.

| All rain | BB rain | Convective | NBB common |
|---|---|---|---|
| | EWN | | |
| $Z_e = 213R^{1.70}$ ($Z_e$–$R$ NMAD = 37%); $R = 0.0120Z_e^{0.86}Z_{dr}^{-3.4}$ ($R$–$Z_eZ_{dr}$ NMAD = 18%); $Z_{DR} = 4.73 \times 10^{-5}Z_e^{1.77}$; $R = 42.0K_{DP}^{0.77}$ ($R$–$K_{DP}$ NMAD = 21%) | $Z_e = 253R^{1.71}$ ($Z_e$–$R$ NMAD = 31%); $R = 0.0097Z_e^{0.88}Z_{dr}^{-3.3}$ ($R$–$Z_eZ_{dr}$ NMAD = 15%); $Z_{DR} = 6.37 \times 10^{-5}Z_e^{2.72}$; $R = 42.2K_{DP}^{0.81}$ ($R$–$K_{DP}$ NMAD = 18%) | $Z_e = 203R^{1.65}$ ($Z_e$–$R$ NMAD = 30%); $R = 0.0093Z_e^{0.89}Z_{dr}^{-3.4}$ ($R$–$Z_eZ_{dr}$ NMAD = 14%); $Z_{DR} = 5.64 \times 10^{-5}Z_e^{2.69}$; $R = 41.3K_{DP}^{0.75}$ ($R$–$K_{DP}$ NMAD = 18%) | $Z_e = 90R^{1.60}$ ($Z_e$–$R$ NMAD = 29%); $R = 0.047Z_e^{0.72}Z_{dr}^{-3.4}$ ($R$–$Z_eZ_{dr}$ NMAD = 17%); $Z_{DR} = 3.19 \times 10^{-5}Z_e^{2.71}$; $R = 51.7K_{DP}^{0.65}$ ($R$–$K_{DP}$ NMAD = 17%) |
| | OFT | | |
| $Z_e = 173R^{1.70}$ ($Z_e$–$R$ NMAD = 33%); $R = 0.0131Z_e^{0.85}Z_{dr}^{-3.3}$ ($R$–$Z_eZ_{dr}$ NMAD = 18%); $Z_{DR} = 4.95 \times 10^{-5}Z_e^{2.73}$; $R = 40.8K_{DP}^{0.73}$ ($R$–$K_{DP}$ NMAD = 20%) | $Z_e = 201R^{1.67}$ ($Z_e$–$R$ NMAD = 27%); $R = 0.0117Z_e^{0.85}Z_{dr}^{-3.0}$ ($R$–$Z_eZ_{dr}$ NMAD = 15%); $Z_{DR} = 7.11 \times 10^{-5}Z_e^{2.65}$; $R = 40.5K_{DP}^{0.75}$ ($R$–$K_{DP}$ NMAD = 16%) | $Z_e = 238R^{1.60}$ ($Z_e$–$R$ NMAD = 26%); $R = 0.0092Z_e^{0.90}Z_{dr}^{-3.7}$ ($R$–$Z_eZ_{dr}$ NMAD = 13%); $Z_{DR} = 5.80 \times 10^{-5}Z_e^{2.71}$; $R = 40.0K_{DP}^{0.73}$ ($R$–$K_{DP}$ NMAD = 16%) | $Z_e = 86R^{1.65}$ ($Z_e$–$R$ NMAD = 30%); $R = 0.050Z_e^{0.72}Z_{dr}^{-3.9}$ ($R$–$Z_eZ_{dr}$ NMAD = 16%); $Z_{DR} = 3.27 \times 10^{-5}Z_e^{2.70}$; $R = 46.5K_{DP}^{0.65}$ ($R$–$K_{DP}$ NMAD = 17%) |
| | HKS | | |
| $Z_e = 174R^{1.69}$ ($Z_e$–$R$ NMAD = 34%); $R = 0.0109Z_e^{0.87}Z_{dr}^{-3.5}$ ($R$–$Z_eZ_{dr}$ NMAD = 17%); $Z_{DR} = 4.41 \times 10^{-5}Z_e^{2.76}$; $R = 40.5K_{DP}^{0.72}$ ($R$–$K_{DP}$ NMAD = 22%) | — | — | — |




FIG. 5. S-band $Z_e$–$R$ relations for convective and (a) BB and (b) common NBB rain types derived using DSDs measured at the EWN and OFT sites. WSR-88D default relations are also shown for comparison.

53-dB$Z$ reflectivity value is often considered to be a threshold for hail detection). For each rain-rate estimator, Table 2 also shows values of the normalized mean absolute difference (NMAD), which is defined as

$$\text{NMAD} = \langle |R_D - R_E| \rangle / \langle R_D \rangle \times 100\%, \qquad (1)$$

where $R_D$ and $R_E$ are rain rates measured by the disdrometer and calculated using a particular estimator, respectively, and angle brackets indicate averaging over all data points. The NMAD value characterizes the data scatter with respect to the best-fit relation and serves as a measure of the estimator "quality" for a given dataset.

Also relatively close are $Z_e$–$R$ relations for BB and convective rains even though convective-core rainfall is characterized by significantly higher mean reflectivities and rain rates when compared with BB rain (see data in Table 1 and Fig. 3). Because of general nonlinearity of the $Z_e$–$R$ relations, mean values of rain rate and reflectivity do not exactly correspond to each

other according to these relations. A relative similarity of BB-rain and convective-rain relations can be explained, in part, by the similarity of their typical DSD spectra shapes (but not the actual drop counts), as discussed in the previous section. Observed convective-rain DSDs have higher drop counts for both smaller and larger drops than do BB-rain DSDs. It results in an increase of both $Z_e$ and $R$, and therefore the resulting $Z_e$–$R$ relations are not widely different for these rain types.

For the reflectivity interval $40 < Z_e < 53$ dB$Z$ (i.e., a typical reflectivity range for convective rain), $R$ estimates from convective-rain $Z_e$–$R$ relations derived for both observational sites are generally higher by about 10%–20% than those obtained from the BB-rain $Z_e$–$R$ relations (Fig. 5). This is similar to the WSR-88D default convective-relation and stratiform-relation difference, which, for this reflectivity interval, varies approximately between 5% and 30%. Some larger differences between convective-rain and BB-rain $Z_e$–$R$ relations for tropical regions were reported previously (e.g., Tokay and Short 1996; Atlas et al. 1999; Thompson et al. 2015). Weak, shallow convection was part of the convective-rain category in some of these previous studies.

The WSR-88D default stratiform relation $Z_e = 200R^{1.6}$, which is used operationally (e.g., Zhang et al. 2011), approximates BB-rain and convective-rain relations for the EWN and OFT sites relatively well (Fig. 5a), even though some average rainfall overestimation can be expected when using this default relation (e.g., about 10% and 20% for reflectivities of 30 and 50 dB$Z$, respectively). The WSR-88D default convective relation ($Z_e = 300R^{1.4}$), however, provides more significant mean overestimation (e.g., ~40% for convective rainfall observed at a 50-dB$Z$ reflectivity level). Between approximately the 30- and 45-dB$Z$ reflectivities these two default WSR-88D relations provide rain-rate estimates that are within approximately 10% of each other.

The common NBB rain, which is not differentiated by the WSR-88D QPE approaches as a separate rain type, is characterized by markedly different $Z_e$–$R$ relations than both convective and BB rainfall (Fig. 5b). Although the exponents $b$ in the $Z_e = aR^b$ relations for all rain types are similar (~1.6–1.7), the prefactors $a$ for common NBB rain are smaller by about a factor of 2.5 than those for other rain types (see Table 2). This is primarily due to the larger fraction of smaller drops in the common NBB rain (relative to other rain types). It results in reflectivities for this rain type being on average about 3–4 dB smaller than those for BB (or convective) rain of similar intensity and is manifested by a shift of common NBB-rain relations relative to other relations as seen in Fig. 5b. When the WSR-88D standard stratiform-rain relation is used for QPE in common NBB rain (which would be the case when rain is not classified as convective or warm using existing segregation approaches), an underestimation of rain rate by about 40% can be expected given that other factors [e.g., a vertical profile of reflectivity (VPR), radar calibration, and beamfilling issues] are adequately addressed. Significant underestimation is also expected if the WSR-88D warm-rain relation is used for typical common NBB-rain reflectivities (e.g., ~35% at 30 dB$Z$).

Similar distinctions between common NBB-rain and BB-rain $Z_e$–$R$ relations were observed in cold-season California rains (Martner et al. 2008). These authors suggested that restrained growth of hydrometeors (i.e., larger fractions of smaller drops) during NBB-rain periods may be a result of orographically forced condensation and coalescence processes. Results obtained here suggest that the NBB rain is also regularly observed in other geographical areas, including those with flat topography (e.g., the EWN site) where orographic effects are not expected to play a significant role.

## 4. Polarimetric rain-rate estimators for different rain types

The $Z_e$–$R$ relations have been used for deriving radar-based QPE for a number of decades (e.g., Doviak and Zrnić 1993). Although reflectivity-based relations remain a viable option for deriving radar-based QPE, a recent polarization upgrade of the WSR-88D network provides opportunities for quantitative use of newly available polarimetric radar variables when retrieving rain rates. These new variables primarily include differential reflectivity $Z_{\rm dr}$, which represents the linear ratio of reflectivities at horizontal and vertical polarizations and is measured directly, and the specific differential phase shift $K_{\rm DP}$, which is derived from measurements of differential phase between horizontally and vertically polarized radar signals. The use of $Z_e$–$Z_{dr}$ measurements provides an additional constraint when compared with reflectivity-only measurements, which can lead to more accurate rain-rate estimates. Polarimetric estimators used with WSR-88D measurements are conventionally expressed as power-law relations (e.g., Bringi and Chandrasekar 2001):

$$R = cZ_e^d Z_{\rm dr}^f \quad \text{and} \tag{2}$$

$$R = gK_{\rm DP}^h, \tag{3}$$

where $R$ is in millimeters per hour, $Z_e$ is in mm$^6$ m$^{-3}$, and positive values of $K_{\rm DP}$ are in degrees per kilometer. The dimensionless ratio $Z_{\rm dr}$ can be simply expressed in terms

of the traditional logarithmic unit differential reflectivity: $Z_{DR}$ (dB) = $10\log_{10}(Z_{dr})$.

*a. $R(Z_e, Z_{dr})$ estimators*

Since values of differential reflectivity in rain are related to the characteristic drop size, such as the mass-weighted drop size or the median volume drop size (e.g., Seliga and Bringi 1976), $Z_{dr}$ constraints could lead to improvements of radar-based QPE even though there is a certain statistical correspondence between $Z_e$ and $Z_{dr}$ values. These values are also related on average because heavier rainfall is usually associated with larger drops. Figure 6 illustrates $Z_{DR}$–$Z_e$ relations where calculations of reflectivity and differential reflectivity using DSDs for all rain types observed at the EWN and OFT sites are shown. Table 2 also shows best power-law fits for these relations obtained for different rain types.

Although different drop mean aspect ratio assumptions cause very little relative change in calculated $Z_e$ values, they affect $Z_{DR}$ values to a stronger degree. To illustrate the sensitivity of differential reflectivity calculations to the assumption of drop shapes, in addition to the data obtained with the Brandes et al. (2005) drop aspect ratios, Figs. 6a and 6b also show calculations using results from another experimental study of drop mean aspect ratio–size correspondence from Thurai et al. (2007). As can be seen from these figures, the drop-shape model sensitivity is relatively modest, and the best $Z_{DR}$–$Z_e$ power-law fits derived using the Brandes et al. (2005) and Thurai et al. (2007) drop mean aspect ratio–drop size models (i.e., the black and pink curves in Figs. 6a and 6b) are close. The $Z_e$–$Z_{DR}$ scatterplots for the DSD data from EWN and OFT are very similar, with their respective differences in the $Z_{DR}$–$Z_e$ fits being generally within 0.2 dB.

The $R(Z_e, Z_{dr})$ estimator in Eq. (2), which has been used with WSR-88D polarimetric measurements, has coefficients $c = 0.0067$, $d = 0.93$, and $f = -3.43$ (Berkowitz et al. 2013). These particular coefficient values found in Bringi and Chandrasekar (2001, section 8.1.1) were obtained using **T**-matrix simulations for assumed theoretical gamma-function DSDs with independently varying parameters of this function (i.e., the gamma-function shape parameter, the median volume drop diameter, and the gamma-function "intercept" parameter). Interdependencies of different gamma-function parameters, however, might exist as indicated by analyses of observed DSDs (Brandes et al. 2003). Also natural DSD ensembles have certain statistical properties (e.g., correlations, means as in Fig. 3, and standard deviations) that are generally not accounted for when gamma-function parameters are varied independently within a predetermined range of their possible variability. In this study, the coefficients in Eq. (2) were obtained using experimentally measured DSD spectra rather than modeled ones.

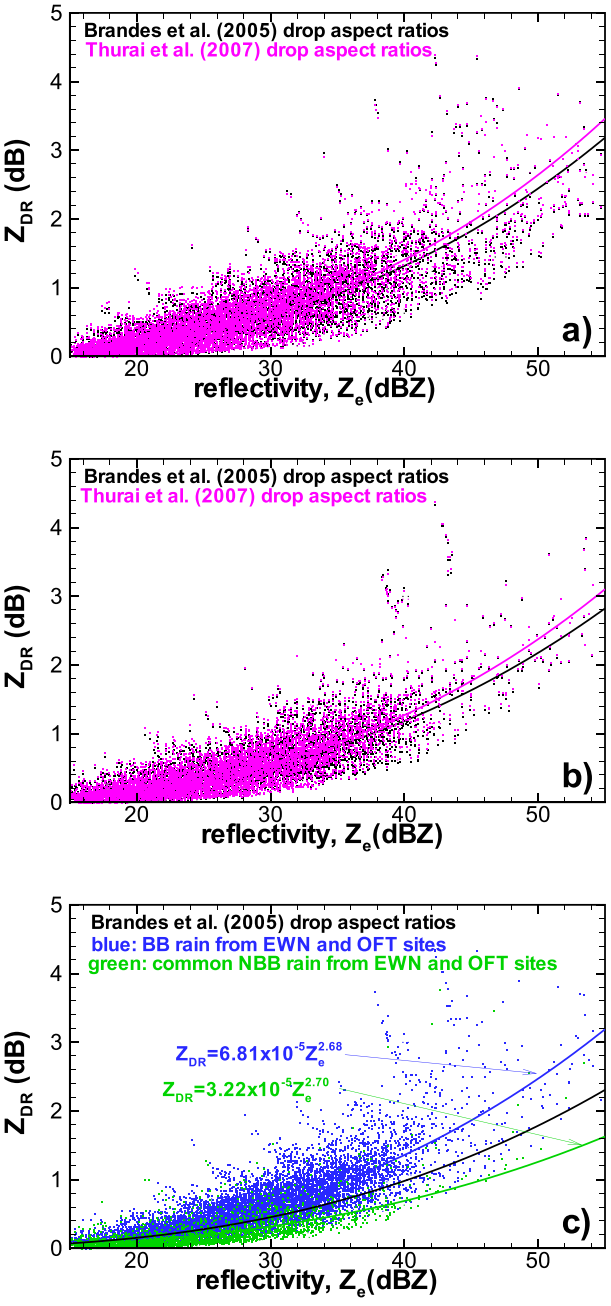


FIG. 6. Scatterplots of S-band differential reflectivity–horizontal polarization reflectivity and corresponding power-law best fits calculated using (a) EWN and (b) OFT site all-rain DSDs. (c) The combined EWN and OFT data scatterplot for BB and common NBB rain obtained using the Brandes et al. (2005) drop mean aspect ratios. The black line in (c) shows results from Eq. (4).

Rain-type-dependent $R(Z_e, Z_{dr})$ estimators were derived using the least squares multiple regression analysis and 1 year of Parsivel DSD spectra data from different

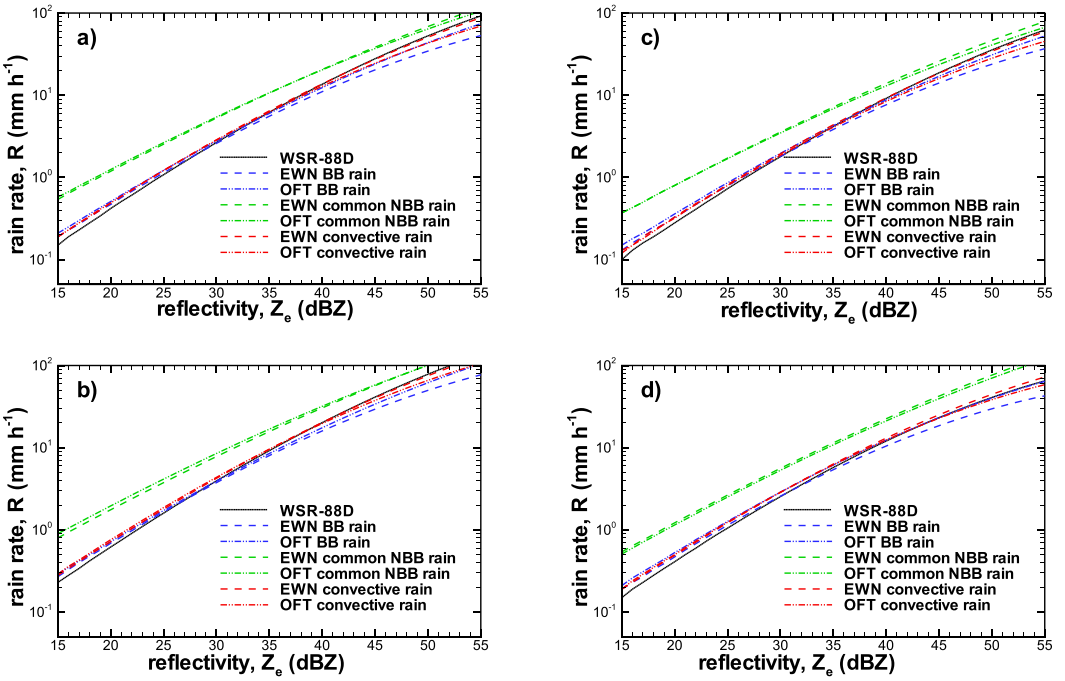


FIG. 7. Rain rates obtained from the S-band $R(Z_e, Z_{dr})$ estimators as a function of reflectivity for (a), (d) mean expected $Z_{DR}$ for all rain types and for mean expected $Z_{DR}$ (b) decreased and (c) increased by 0.5 dB. Here (a)–(c) are for the Brandes et al. (2005) drop mean aspect ratio model, and (d) is for the Thurai et al. (2007) drop mean aspect ratio model.

HMT-Southeast observational sites. The respective rain-rate estimators are shown in Table 2 with coefficients derived using the Brandes et al. (2005) mean spheroidal drop aspect ratio–size relation. Because of noisiness of differential reflectivity measurements, the use of $R(Z_e, Z_{dr})$ estimators could be more practical for moderate and heavier rainfall when $Z_{DR}$ values are not too small (i.e., drops are not too spherical), and therefore Table 2 shows statistical parameters of these estimators corresponding to $R > 5\,\text{mm h}^{-1}$.

To better visualize these estimators and understand differences among them, Figs. 7a–c present $R$ values calculated using $R(Z_e, Z_{dr})$ estimators from Table 2 as a function of reflectivity $Z_e$ for different types of rain. To assess the impact of $Z_{dr}$ as a second radar variable influencing estimates of rain rate in events of typical (for a given $Z_e$), lower, and higher differential reflectivity values, Fig. 7a shows $R$ estimates when a typical expected $Z_{DR}$ value corresponding to the best power-law $Z_{DR}$–$Z_e$ fits from Table 2 is assumed, and Fig. 7b (Fig. 7c) shows data when this best-fit $Z_{DR}$ value is decreased (increased) by 0.5 dB. A 0.5-dB $Z_{DR}$ value represents a scatter of differential reflectivities around the best $Z_{DR}$–$Z_e$ fit. Figure 7d depicts the data for typical $Z_{dr}$ values but using $R(Z_e, Z_{dr})$ estimators with coefficients (not shown in Table 2) derived assuming the Thurai et al. (2007) drop mean aspect ratios rather than those derived using the Brandes et al. (2005) drop-shape results.

Comparison of Figs. 7a and 7d allows assessment of the drop aspect ratio assumption on rain-rate estimates. It can be seen that this assumption (between the two aspect ratio models considered here) has only minor impact on the results when reflectivity varies in a relatively large interval from ~20 to ~45 dB$Z$. Comparisons of Figs. 7a–c with Figs. 5a and 5b, which are presented for the same axis intervals, indicate that QPE results obtained with rain-type-dependent $Z_e$–$R$ relations are expected to generally be within those derived using $R(Z_e, Z_{dr})$ estimators for corresponding rain types when $Z_{DR}$ varies within approximately ±0.5 dB from the expected (for given a $Z_e$) value.

It can also be seen from Fig. 7 that, similar to $Z_e$–$R$ relations, the common NBB-rain $R(Z_e, Z_{dr})$ estimators differ noticeably from those for convective and BB rain types. The use of the default $R = 0.0067 Z_e^{0.93} Z_{dr}^{-3.43}$ WSR-88D estimator provides generally satisfactory results for those latter rain types, but it will result in QPE underestimation by as much as a factor of ~2 when common NBB rain is observed. The underestimation is expected to be greater for lower reflectivities (e.g., $Z_e \leq$ 35 dB$Z$). The $R(Z_e, Z_{dr})$ estimators for the BB and convective rain types provide close results, and there is no significant dependence on which observational-site

DSDs are used for deriving coefficients in these estimators. As seen from Fig. 7, there is no significant difference between $R(Z_e, Z_{dr})$ estimators for BB and convective rain types, at least for reflectivities less than ~45 dB$Z$.

### b. $R(K_{DP})$ estimators

Rainfall retrieval using specific differential phase shift $K_{DP}$ is another polarimetric radar approach that has been used with WSR-88D measurements. This approach has a number of practical advantages (Zrnić and Ryzhkov 1996), which include independence of radar absolute calibration, immunity to partial beam blockage and ground clutter canceling, and ease of isolating effects of anomalous propagation. The main disadvantage of this rain-retrieval approach at S-band radar frequencies is that $K_{DP}$ values are generally small and often noisy when derived using conventional filtering approaches (e.g., Hubbert and Bringi 1995) for lighter rainfall, and therefore their practical use for such rainfall is often limited except when applied at higher radar frequencies (e.g., Matrosov et al. 2002, 2006). These approaches, however, are useful for heavier rainfall, and especially for deriving rain rates in rain–hail mixtures (e.g., Balakrishnan and Zrnić 1990; Matrosov et al. 2013). WSR-88D use of $R(K_{DP})$ estimators includes estimating $R$ in such mixtures using the estimator Eq. (3) with $g = 44.0$ and $h = 0.822$ (Berkowitz et al. 2013).

Table 2 shows the $R(K_{DP})$ estimators obtained using calculations with the DSDs observed at the HMT-Southeast sites and assuming the Brandes et al. (2005) drop aspect ratios. The coefficients $g$ and $h$ in the best power-law relations in Eq. (3) and the corresponding NMAD values were derived for the drop spectra that were characterized by $K_{DP}$ values of greater than a threshold of $0.1^\circ\,km^{-1}$. At this threshold, values of specific differential phase shift obtained from differential phase shift measurements at S band using filtering approaches are generally reliable (Matrosov et al. 2006), although smaller $K_{DP}$ values could also be used in practice when some additional averaging and special $K_{DP}$ derivation approaches are applied (e.g., Lim et al. 2013). For the DSD dataset from this study, the number of DSD spectra for which theoretical $K_{DP} > 0.1^\circ\,km^{-1}$ is about 8%, 38%, and 5% of the total amount DSD spectra with $Z_e > 15$ dB$Z$, for BB, convective NBB, and common NBB rain, respectively. The choice of the drop aspect ratio model [i.e., Brandes et al. (2005) aspect ratio–drop size relation vs the one from Thurai et al. (2007)] results only in very minor changes of the coefficients in the $R(K_{DP})$ estimators. For different types of rain, the respective changes in the prefactor $g$ values are generally within 5%, and the exponent $h$ varies within 0.01 from the values shown in Table 2. Figure 8 shows $R$–$K_{DP}$ scatterplots for all rain DSDs observed at EWN, OFT, and HKS. It can be seen that the amount of data scatter and best power-law fit are very similar at all the sites.

Figure 9 provides graphical comparisons of the $R(K_{DP})$ estimators obtained for various rain types and different observational sites. As with other rain-rate estimators, which were discussed previously, there are no significant differences between estimators for the same rain type derived from DSDs measured at the EWN and OFT observational sites, even though the $K_{DP}$ thresholding reduces the number of data points. As before, the estimators for BB and NBB convective rain provide similar results. The WSR-88D estimator also provides rain-rate values that are generally close to the ones from BB-rain and convective-rain estimators from both observational sites when $0.1^\circ < K_{DP} < 2^\circ\,km^{-1}$, which corresponds to rain rates between approximately 7 and 70 mm $h^{-1}$.

The coefficients in the $R(K_{DP})$ estimators for common NBB rain type are very different from those for other relations in Table 2, which, in part, is due to the fact that this rain type contains larger fractions of more spherical smaller drops (as compared with larger drops that are more nonspherical). The use of relations derived for BB or convective rain (and also the WSR-88D relation) can cause some significant underestimation of common NBB rain rate for smaller $K_{DP}$ values (e.g., a greater than 30% underestimation for $K_{DP} < 0.3^\circ\,km^{-1}$). The relative separation of the common NBB-rain $R(K_{DP})$ power-law fits from the fits for the other rain types, however, is smaller than in the cases of the $Z_e$–$R$ and $R(Z_e, Z_{dr})$ estimators. This is due, in part, to the fact that $K_{DP}$ is approximately proportional to the lower DSD moment (e.g., Zrnić and Ryzhkov 1996; Matrosov et al. 2006), and therefore the moment disparity is not as large as for the $Z_e$ and $R$ pair (i.e., ~6 for $Z_e$ and approximately ~3.67 for $R$) and specific-phase–rain-rate relations are less susceptible to DSD details than are relations that contain reflectivity. As seen from Table 2, NMAD values for $K_{DP}$-based estimators are very close those for $R(Z_e, Z_{dr})$ estimators and are smaller than those for $Z_e$–$R$ relations. This result suggests that in their range of applicability the polarimetric estimators are potentially more accurate than the traditional reflectivity-based approaches (given that polarimetric radar variables are reliably measured).

## 5. Potential for using polarimetric data to differentiate between BB and common NBB rain

As shown in section 2, common NBB rain is characterized by DSDs that, because of a larger fraction of

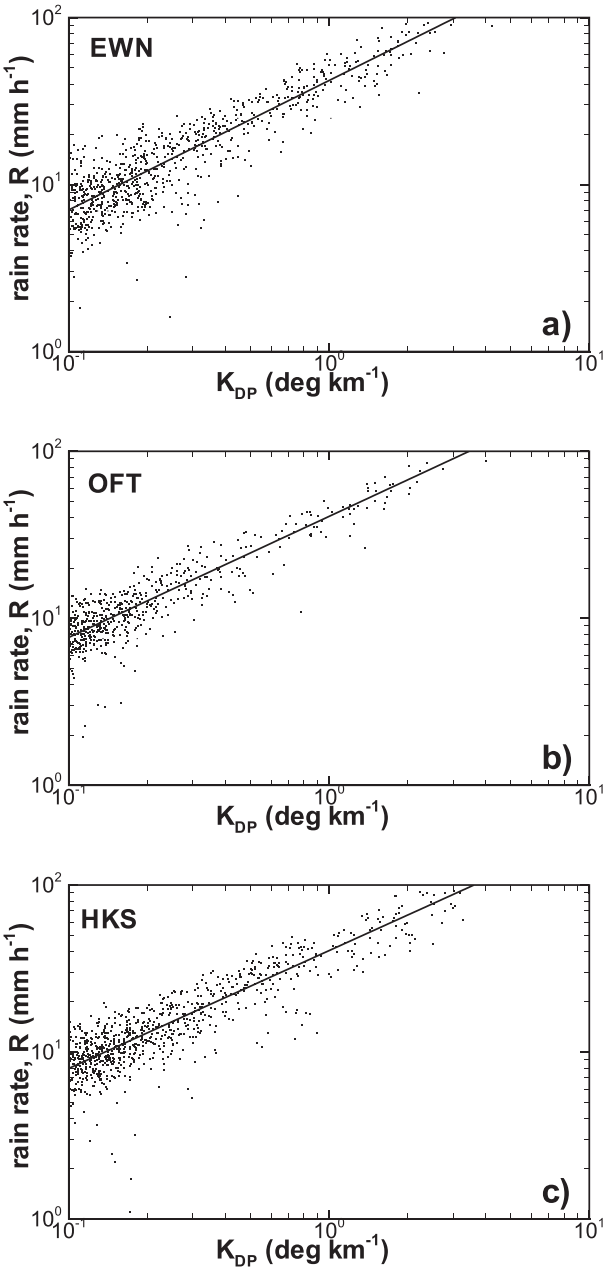


FIG. 8. S-band $R$–$K_{DP}$ scatterplots for all rain DSDs with $K_{DP} > 0.1°\ km^{-1}$ observed at the (a) EWN, (b) OFT, and (c) HKS sites. Brandes et al. (2005) drop mean aspect ratios were used in calculations.

smaller drops, are markedly different from those characteristic of other rain types. This difference results in significant differences in the coefficients for radar-based rain estimators for this rain type, which could lead to substantial underestimation of radar-based QPE if inappropriate or default estimators are used when observing common NBB rain. Given this situation, algorithms are needed to identify this rain type so that appropriate estimators can be used.

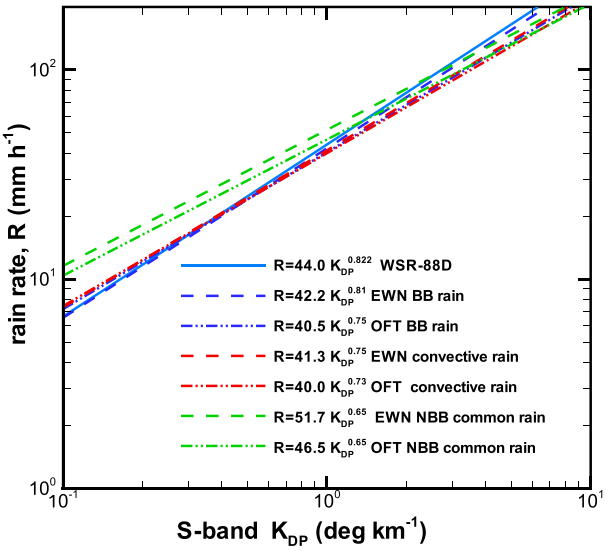


FIG. 9. Best-fit power-law $R$–$K_{DP}$ relations obtained using DSDs observed at the EWN and OFT sites for different rain types.

Current radar-based rain-type identification algorithms, including those used with the WSR-88D measurements (e.g., Steiner et al. 1995; Penide et al. 2013; Qi et al. 2013), are mostly aimed at differentiating stratiform rainfall, which often exhibits the radar bright band, and areas of heavier convective precipitation. Convective–stratiform differentiation is important because applying VPR corrections for BB stratiform rain at farther ranges is essential, even though coefficients in the radar rain-rate estimators for these rain types could be similar. Identifying areas of common NBB rain is important for appropriate rain-rate estimators to be applied when deriving more accurate radar-based QPE.

One polarimetric radar approach, which can be suggested for identifying common NBB rain in the precipitation areas outside of convective cores, is based on analyzing observed $Z_{DR}$–$Z_e$ patterns. Figure 6c depicts combined $Z_{DR}$–$Z_e$ scatterplots for BB and common NBB rain obtained from DSDs observed at the EWN and OFT measurement sites. It can be seen from the best power-law fits shown in this figure that, for a given value of reflectivity, typical differential reflectivity values in BB rain are larger by more than a factor of 2 (in logarithmic scale units) than those in common NBB rain. The mean threshold differential reflectivity value $Z_{DR}^{(t)}$, essentially separating the $Z_{DR}$–$Z_e$ distributions for BB and common NBB rain types, can be obtained from the two power-law best fits for these rain types in Fig. 6c as

$$Z_{DR}^{(t)}\ (\mathrm{dB}) \approx 0.000\,048 Z_e^{2.69}\ (\mathrm{dB}Z). \qquad (4)$$

For the Brandes et al. (2005) drop mean aspect ratios, about 80% of BB-rain data points in Fig. 6c have

$Z_{DR} > Z_{DR}^{(t)}$ while approximately the same amount (i.e., ~80%) of common NBB-rain data points are characterized by $Z_{DR} \leq Z_{DR}^{(t)}$. For the Thurai et al. (2007) drop mean aspect ratios, the corresponding numbers change by only a few percentage points. This simple approach, however, is appropriate when radar echoes come primary from rainfall so that there is no significant contamination from melting and ice hydrometeors.

## 6. Discussion and conclusions

Earlier studies (Martner et al. 2008) showed that a significant fraction of cool-season rainfall in the U.S. West Coast regions does not exhibit a radar bright band. These authors suggested a linkage between this nonbrightband rain and orographically forced rainfall-formation processes in shallower clouds. NBB rain is characterized by DSDs with higher relative amounts of smaller drops when compared with brightband rain. This situation results in NBB $Z_e$–$R$ relations being distinct from those used in operational algorithms, which can lead to underestimation of precipitation amounts for this rain type derived using existing radar-based QPE schemes. The use of inappropriate rain-rate estimators is an important factor (although not the only one) affecting accuracy of radar-based precipitation retrievals.

Results of this study, which was conducted using yearlong collocated measurements of S-band profiler and Parsivel disdrometer DSDs, showed that NBB rain is also often observed at the southeastern HMT-SEPS sites at New Bern and Old Fort. This common NBB rain is distinct from deep-convective NBB rain, which is usually considered and segregated as a special rain type when applying different operational radar-based QPE approaches. The radar echo tops of common NBB rain can extend above the environmental freezing level, and this rain type can also result from shallow convection lacking the strong convective core that could be identified by operational radar-based classification algorithms. Common NBB rain amounts to about 20% of the total precipitation accumulation in the study area and is observed not only in the mountainous terrain at OFT but also in the relatively flat coastal area at EWN where orographically forced rainfall formation processes are not expected.

Because of larger fractions of smaller drops, common NBB rain has radar-based rain-rate estimators that are distinct from those of other rain types, including ones based on traditional $Z_e = aR^b$ relations as well as the polarimetric radar estimators that make use of differential reflectivity $Z_{DR}$ and specific differential phase shift $K_{DP}$. S-band estimators applicable to WSR-88D measurements were considered in this study. The exponents $b$ in the traditional relations for all rain types were similar (~1.6–1.7), but the prefactors for common NBB rain were smaller by approximately a factor of 2.5 than those for other rain types, which could result in precipitation underestimation by approximately 40% if relations for BB or convective rain are used. This amount of underestimation would be quantitatively similar to the effect if the radar absolute calibration biases were about −3.5 dB or to the effect of partial beamfilling of about 45%. These two latter rain types were characterized by similar $Z_e$–$R$ relations that were relatively well approximated by the WSR-88D default stratiform relation $Z_e = 200R^{1.60}$. None of the default WSR-88D $Z_e$–$R$ relations satisfactorily describe common NBB rain.

Similar to the $Z_e$–$R$ relations, polarimetric $R(Z_e, Z_{dr})$ and $R(K_{DP})$ estimators for BB and convective rain were close, providing rain-rate estimates mostly within ~15% in the 20–45-dB$Z$ reflectivity range [for $R(Z_e, Z_{dr})$ estimators] and ~10% for differential phase shifts smaller than $0.1^\circ\,km^{-1}$ [for $R(K_{DP})$ estimators]. The polarimetric estimators previously utilized with WSR-88D measurements (i.e., $R = 0.0067Z_e^{0.93}Z_{dr}^{-3.43}$ and $R = 44K_{DP}^{0.822}$) provide rain rates that were generally within the same margins of variability for these rain types. The polarimetric estimators for common NBB rain, however, are distinct, and the use of other rain-type or WSR-88D estimators can cause significant underestimation of radar-based QPE for this rain type. The degree of this underestimation is greater for $R(Z_e, Z_{dr})$ and can be larger than a factor of 2 for rainfall with lower reflectivities (e.g., $Z_e < 30$ dB$Z$). Because the relations between differential phase shift and rain rate are less susceptible to DSD variations when compared with estimators containing $Z_e$, the $R(K_{DP})$ estimator underestimation is generally smaller but is still appreciable for $K_{DP} < 1^\circ\,km^{-1}$ (e.g., ~30% at $K_{DP} \approx 0.3^\circ\,km^{-1}$). Derived from experimentally observed DSDs, $Z_{DR}$ and $K_{DP}$ values exhibit only very modest sensitivity to different drop aspect ratio–size relations that are often used by the radar-meteorology community.

Traditional nonpolarimetric radar $Z_e$–$R$ relations as well as polarimetric $R(Z_e, Z_{dr})$ and $R(K_{DP})$ relations derived for the same rain types using DSDs observed at different HMT-Southeast sites were very similar despite a significant site separation (~470 km) and differing terrain. This result might suggest some generality of the derived rain-rate estimators for a larger area. The results of this study are also in general agreement with findings by Martner et al. (2008), who also found that nonconvective NBB-rain $Z_e = aR^b$ relations or winter-type rainfall in California is characterized by

significantly lower coefficients $a$ relative to the case for BB rain. Their values for $a$ varied between 44 and 77, and the exponents $b$ were between 1.65 and 1.9.

Since common NBB rain frequently occurs in different geographic areas and has radar rain-rate estimators that are distinct from those of other rain types, it is important to distinguish it from other rain types. Existing operational radar rain-type segregation schemes usually differentiate between convective-core rain and stratiform rain, which often exhibits the radar bright band, but do not identify common NBB rain. S-PROF observations from HMT-SEPS show that periods of common NBB rain, which is observed outside of deep-convection periods, often interlace with periods of BB rain. The NBB rain, however, can be potentially identified using polarimetric $Z_e$–$Z_{DR}$ measurements. As the results of this study indicate, this rain type has distinct $Z_e$–$Z_{DR}$ patterns, which can be used for prospective techniques to separate areas of NBB and BB rain. Future validation and testing of common NBB-rain segregation techniques should be based on closely collocated WSR-88D polarimetric measurements and robust identification of rain type from vertically pointing radar-profiler observations.

*Acknowledgments.* This work has been supported by the NOAA Office of Weather and Air Quality U.S. Weather Research program and the Physical Sciences Division at the NOAA Earth System Research Laboratory. The authors are grateful to the PSD scientists and engineers who deployed the instruments and collected and quality controlled the high-quality data as part of HMT-SEPS.

## REFERENCES

Adirosi, E., E. Gorgucci, L. Baldini, and A. Tokay, 2014: Evaluation of gamma raindrop size distribution assumption through comparison of rain rates of measured and radar-equivalent gamma DSD. *J. Appl. Meteor. Climatol.*, **53**, 1618–1635, doi:10.1175/JAMC-D-13-0150.1.

——, L. Baldini, F. Lombardo, F. Russo, F. Napolitano, E. Volpi, and A. Tokay, 2015: Comparison of different fittings of drop spectra for rainfall retrievals. *Adv. Water Resour.*, **83**, 55–67, doi:10.1016/j.advwatres.2015.05.009.

Atlas, D., C. W. Ulbrich, F. D. Marks Jr., E. Amitai, and C. R. Williams, 1999: Systematic variation of drop size and radar–rainfall relations. *J. Geophys. Res.*, **104**, 6155–6169, doi:10.1029/1998JD200098.

Balakrishnan, N., and D. S. Zrnić, 1990: Estimation of rain and hail rates in mixed-phase precipitation. *J. Atmos. Sci.*, **47**, 565–583, doi:10.1175/1520-0469(1990)047<0565:EORAHR>2.0.CO;2.

Berkowitz, D. S., J. A. Schultz, S. Vasiloff, K. L. Elmore, C. D. Payne, and J. B. Boettcher, 2013: Status of dual pol QPE in the WSR-88D network. *Proc. 27th Conf. on Hydrology*, Austin, TX, Amer. Meteor. Soc., 2.2. [Available online at https://ams.confex.com/ams/93Annual/webprogram/Manuscript/Paper221525/AMS27thHydro_2.2Berkowitz_et_al.pdf.]

Brandes, E. A., G. Zhang, and J. Vivekanandan, 2003: An evaluation of a drop distribution–based polarimetric radar rainfall estimator. *J. Appl. Meteor.*, **42**, 652–660, doi:10.1175/1520-0450(2003)042<0652:AEOADD>2.0.CO;2.

——, ——, and ——, 2005: Corrigendum. *J. Appl. Meteor.*, **44**, 186, doi:10.1175/1520-0450(2005)44<186:C>2.0.CO;2.

Bringi, V. N., and V. Chandrasekar, 2001: *Polarimetric Doppler Weather Radar.* Cambridge University Press, 636 pp.

Doviak, R. J., and D. S. Zrnić, 1993: *Doppler Radar and Weather Observations.* Academic Press, 562 pp.

Ekerete, K.'u.-M. E., F. H. Hunt, J. L. Jeffery, and I. E. Otung, 2015: Modeling rainfall drop size distribution in southern England using a Gaussian mixture model. *Radio Sci.*, **50**, doi:10.1002/2015RS005674.

Hubbert, J., and V. N. Bringi, 1995: An iterative filtering technique for the analysis of copular differential phase and dual-frequency radar measurements. *J. Atmos. Oceanic Technol.*, **12**, 643–648, doi:10.1175/1520-0426(1995)012<0643:AIFTFT>2.0.CO;2.

Huschke, R. E., Ed., 1959: *Glossary of Meteorology*. Amer. Meteor. Soc., 638 pp.

Lim, S., R. Cifelli, V. Chandrasekar, and S. Y. Matrosov, 2013: Precipitation classification and quantification using X-band dual-polarization radar: Application in the Hydrometeorology Testbed. *J. Atmos. Oceanic Technol.*, **30**, 2108–2120, doi:10.1175/JTECH-D-12-00123.1.

Löffler-Mang, M., and J. Joss, 2000: An optical disdrometer for measuring size and velocity of hydrometeors. *J. Atmos. Oceanic Technol.*, **17**, 130–139, doi:10.1175/1520-0426(2000)017<0130:AODFMS>2.0.CO;2.

Marshall, J. S., W. Hitschfeld, and K. L. S. Gunn, 1955: Advances in radar weather. *Advances in Geophysics*, Vol. 2, H. E. Landsberg, Ed., Academic Press, 1–56, doi:10.1016/S0065-2687(08)60310-6.

Martner, B. E., S. E. Yuter, A. B. White, S. Y. Matrosov, D. E. Kingsmill, and F. M. Ralph, 2008: Raindrop size distributions and rain characteristics in California coastal rainfall for periods with and without a radar bright band. *J. Hydrometeor.*, **9**, 408–425, doi:10.1175/2007JHM924.1.

Matrosov, S. Y., 2005: Attenuation-based estimates of rainfall rates aloft with vertically pointing $K_a$-band radars. *J. Atmos. Oceanic Technol.*, **22**, 43–54, doi:10.1175/JTECH-1677.1

——, K. A. Clark, B. E. Martner, and A. Tokay, 2002: X-band polarimetric radar measurements of rainfall. *J. Appl. Meteor.*, **41**, 941–952, doi:10.1175/1520-0450(2002)041<0941:XBPRMO>2.0.CO;2.

——, R. Cifelli, P. C. Kennedy, S. W. Nesbitt, S. A. Rutledge, V. N. Bringi, and B. E. Martner, 2006: A comparative study of rainfall retrievals based on specific differential phase shifts at X- and S-band radar frequencies. *J. Atmos. Oceanic Technol.*, **23**, 952–963, doi:10.1175/JTECH1887.1.

——, ——, and D. Gochis, 2013: Measurements of heavy convective rainfall in the presence of hail in flood-prone areas using an X-band polarimetric radar. *J. Appl. Meteor. Climatol.*, **52**, 395–407, doi:10.1175/JAMC-D-12-052.1.

——, F. M. Ralph, P. N. Neiman, and A. B. White, 2014: Quantitative assessment of operational weather radar rainfall estimates over California's northern Sonoma County using HMT-West data. *J. Hydrometeor.*, **15**, 393–410, doi:10.1175/JHM-D-13-045.1.

Penide, G., A. Protat, V. V. Kumar, and P. T. May, 2013: Comparisons of two convective/stratiform precipitation classification techniques: Radar reflectivity texture versus drop size

distribution-based approach. *J. Atmos. Oceanic Technol.*, **30**, 2788–2797, doi:10.1175/JTECH-D-13-00019.1.

Qi, Y., J. Zhang, and P. Zhang, 2013: A real-time automated convective and stratiform precipitation segregation algorithm in native radar coordinates. *Quart. J. Roy. Meteor. Soc.*, **139**, 2233–2240, doi:10.1002/qj.2095.

Rosenfeld, D., D. B. Wolff, and D. Atlas, 1993: General probability-matched relations between radar reflectivity and rain rate. *J. Appl. Meteor.*, **32**, 50–72, doi:10.1175/1520-0450(1993)032<0050:GPMRBR>2.0.CO;2.

Seliga, T. A., and V. N. Bringi, 1976: Potential use of radar differential reflectivity measurements at orthogonal polarizations for measuring precipitation. *J. Appl. Meteor.*, **15**, 69–76, doi:10.1175/1520-0450(1976)015<0069:PUORDR>2.0.CO;2.

Steiner, M., R. A. Houze Jr., and S. E. Yuter, 1995: Climatological characterization of three-dimensional storm structure from radar and rain gauge data. *J. Appl. Meteor.*, **34**, 1978–2007, doi:10.1175/1520-0450(1995)034<1978:CCOTDS>2.0.CO;2.

Thompson, E. J., S. A. Rutledge, B. Dolan, and M. Thurai, 2015: Drop size distributions of convective and stratiform rain over the equatorial Indian and west Pacific Oceans. *J. Atmos. Sci.*, **72**, 4091–4125, doi:10.1175/JAS-D-14-0206.1.

Thurai, M., G. J. Huang, V. N. Bringi, W. L. Randeu, and M. Schönhuber, 2007: Drop shapes, model comparisons, and calculations of radar parameters in rain. *J. Atmos. Oceanic Technol.*, **24**, 1019–1032, doi:10.1175/JTECH2051.1.

——, W. A. Petersen, A. Tokay, C. Achultz, and P. Gatlin, 2011: Drop size distribution comparisons between Parsivel and 2-D video disdrometers. *Adv. Geosci.*, **30**, 3–9, doi:10.5194/adgeo-30-3-2011.

Tokay, A., and D. A. Short, 1996: Evidence from tropical raindrop spectra of the origin of rain from stratiform versus convective clouds. *J. Appl. Meteor.*, **35**, 355–371, doi:10.1175/1520-0450(1996)035<0355:EFTRSO>2.0.CO;2.

Waterman, P. C., 1965: Matrix formulation of electromagnetic scattering. *Proc. IEEE*, **53**, 805–812, doi:10.1109/PROC.1965.4058.

White, A. B., P. J. Neiman, F. M. Ralph, D. E. Kingsmill, and P. O. G. Persson, 2003: Coastal orographic rainfall processes observed by radar during the California Land-Falling Jets Experiment. *J. Hydrometeor.*, **4**, 264–282, doi:10.1175/1525-7541(2003)4<264:CORPOB>2.0.CO;2.

Woodley, W. L., 1970: Precipitation results from a pyrotechnic cumulus seeding experiment. *J. Appl. Meteor.*, **9**, 242–257, doi:10.1175/1520-0450(1970)009<0242:PRFAPC>2.0.CO;2.

Zhang, J., and Coauthors, 2011: National Mosaic and Multi-Sensor QPE (NMQ) system: Description, results, and future plans. *Bull. Amer. Meteor. Soc.*, **92**, 1321–1338, doi:10.1175/2011BAMS-D-11-00047.1.

Zrnić, D. S., and A. Ryzhkov, 1996: Advantages of rain measurements using specific differential phase. *J. Atmos. Oceanic Technol.*, **13**, 454–464, doi:10.1175/1520-0426(1996)013<0454:AORMUS>2.0.CO;2.